$Fe(N_2)_n$ ($n = 1-5$): Structure, Bonding, and Vibrations from Density Functional Theory

Hélio A. Duarte[†] and Dennis R. Salahub*[,‡]

Département de chimie, Université de Montréal, CP 6128, succursale centre-ville, Montréal, Québec H3C 3J7, Canada

Tom Haslett and Martin Moskovits

Department of Chemistry, University of Toronto, 80 St. George Street, Toronto, Ontario M5S 1A1, Canada

Received January 8, 1999

The $Fe(N_2)_n$ ($n = 1-5$) complexes have been studied with the LCGTO-KS-DF method. The structures containing end-on and side-on N_2 ligands have been fully optimized and the dissociation energies estimated. The ground states are predicted to be end-on complexes with the exception of $n = 2$. The vibrational analysis of all predicted ground states is reported. The effect of ^{15}N isotopic substitution on the vibrational frequencies has been estimated. Comparisons are made with the isoelectronic species $Fe(CO)_n$. The Fe−N_2 bonding has been discussed in terms of σ donation and π back-donation and the Mulliken population analysis. The predicted harmonic frequencies show that the infrared spectra of $Fe(N_2)_4$ and $Fe(N_2)_5$ are similar, and the two complexes could not be distinguished in nitrogen matrix experiments using infrared spectroscopy.

Introduction

The interaction of molecular species with transition metals has attracted the attention of both experimentalists and theorists due to its importance in many important biological and industrial processes.[1] The interaction of diatomic molecules, such as CO, NO, N_2, and O_2, with transition metal systems is of great interest for understanding the mechanism of their activation in many catalytic systems.[1,2] The interaction of carbonyls with transition metals has been widely studied theoretically and experimentally.[1,3] CO interacts with transition metals by donating electrons from its 5σ orbital (σ donation) and receiving electron density from the metal d orbitals into the antibonding $2\pi^*$ orbital (π back-donation). The CO bond weakens due to the π back-donation, and the CO stretching frequency decreases compared to free CO. The 5σ and $2\pi^*$ orbitals are largely localized on the carbon atom and projected away from the internuclear bond. However, the isoelectronic species, N_2, is nonpolar and the corresponding orbitals $3\sigma_g$ and $1\pi_g^*$ of N_2 are equally distributed over the two nitrogen atoms. It is expected that the σ donation and π back-donation interactions in M−N_2 are not as efficient as in M−CO complexes. The differences of the spatial distribution of the molecular orbitals in CO and N_2 may explain the differences in the interaction of these molecules with transition metal systems.

The chemisorption of N_2 on metal surfaces has been studied extensively (see, for example, ref 4 and references therein) due to its importance in many catalytic processes. For example, the dissociation of N_2 is the rate-determining step in the synthesis of ammonia using iron as a catalyst;[5] however, the mechanism is still not well understood. Experimentally, it has been shown that dinitrogen bonds to iron dimers in a solid nitrogen matrix.[6] Recently, Haslett et al.[7] detected dinitrogen iron complexes in a nitrogen matrix; however, their geometry and electronic properties have not been elucidated yet. On the other hand, their isoelectronic species $Fe(CO)_n$ have been extensively studied theoretically and experimentally.[8−12] The interaction of nitrogen with the transition metal dimers and atoms has been studied theoretically using CASSCF (complete active space self-consistent-field)[13,14] and LCGTO-KS-DF (linear combination of Gaussian type orbitals−Kohn Sham−density functional)[15−17] methods.

We have studied the $Fe(N_2)_n$ ($n = 1-5$) complexes by means of an LCGTO-KS-DF method. The respective isoelectronic species $Fe(CO)_n$ are invoked for comparison since iron carbonyls have been extensively studied theoretically and experimentally.

[†] Permanent address: Departamento de Quimica, Universidade Federal de Minas Gerais, Av. Antônio Carlos 6627, 31.270-901 Belo Horizonte, MG, Brazil.

[‡] Present address: Steacie Institute for Molecular Sciences, National Research Council Canada, 100 Sussex Drive, Ottawa, Ontario K1A 0R6, Canada.

(1) Russo, N.; Salahub, D. R. Metal-Ligand Interactions−Structure and Reactivity; *NATO ASI Ser., Ser. C* **1996**, 474.
(2) Culotta, E.; Koshland, D. E., Jr. *Science* **1992**, *258*, 1862.
(3) Yates, J. T. *Surf. Sci.*, **1994**, *299/300*, 731.
(4) Rao, C. N. R.; Rao, G. R. *Surf. Sci. Rep.* **1991**, *13*, 223.
(5) Ertl, G. *J. Vac. Sci. Technol.* **1983**, *1*, 1247.
(6) Barrett, P. H.; Montano, P. A. *J. Chem. Soc., Faraday Trans. 2* **1977**, *73*, 378.
(7) Haslett, T.; Moskovits, M.; Duarte, H. A.; Salahub, D. R. Unpublished work.
(8) Poliakoff, M.; Turner, J. J. *J. Chem. Soc., Dalton Trans.* **1977**, 2276.
(9) Barton, T. J.; Grinter, R.; Thomson, A. J.; Davies, B.; Poliakoff, M. *J. Chem. Soc., Chem. Commun.* **1977**, 841.
(10) Ziegler, T.; Tschinke, V.; Ursenbach, C. *J. Am. Chem. Soc.* **1987**, *109*, 4825.
(11) Fournier, R. *J. Chem. Phys.* **1993**, *99*, 1801.
(12) Barnes, L. A.; Rosi, M.; Bauschlicher, C. W., Jr. *J. Chem. Phys.* **1991**, *94*, 2031.
(13) Siegbahn, P. E. M. *J. Chem. Phys.* **1991**, *95*, 364.
(14) Bauschlicher, C. W., Jr.; Petterson, L. G. M.; Siegbahn, P. E. M. *J. Chem. Phys.* **1987**, *87*, 2129.
(15) Zacarias, A.; Torrens, J.; Castro, M. *Int. J. Quantum Chem.* **1997**, *61*, 467.
(16) Chertihin, G. V.; Andrews, L.; Neurock, M. *J. Phys. Chem.* **1996**, *100*, 14609.
(17) Zacarias, A.; Castro, M. *Int. J. Quantum Chem.* **1996**, *60*, 1419.

10.1021/ic990066z CCC: $18.00
Published on Web 07/30/1999

In the present work, the predicted ground state, dissociation binding energies, vibrational frequencies, and the effect of isotopic substitution are reported. The Fe−N_2 bonding in the complexes studied is discussed in terms of the Mulliken population analysis and the σ donation and π back-donation.

Computational Aspects

The $Fe(N_2)_n$ ($n = 1-5$) complexes have been studied using the LCGTO-KS-DF method implemented in the program deMon-KS.[18,19] The generalized gradient approximation (GGA) for the exchange and correlation (XC) functional has been used with the Becke[20] expression for exchange and that of Perdew[21,22] for correlation (GGA-BP). In the study of FeN_2, we have also used the XC functional scheme GGA-PW91 of Perdew and Wang[23,24] and the GGA-PP scheme of Perdew.[21,22,25] The basis sets used in this work were obtained by the procedure described in refs 26 and 27; for the iron atom, it has the contraction pattern (63321/5211*/41+). The auxiliary basis sets used for fitting the density and XC potential have the pattern (5,5;5,5) consisting of five s and five s, p, d shells of functions. The contraction patterns used for nitrogen was (7111/411/1*) (TZVP). The auxiliary basis sets have the pattern (4,3;4,3). The charge density was fitted analytically, and the XC potential was fitted numerically using a grid of 48 radial shells and 26 angular points per shell, giving a total of 1248 points per atom. The complexes have been fully optimized by using the standard Broyden−Fletcher−Goldfarb−Shanno (BFGS) method.[28] The geometries were optimized without symmetry constraints, and hence, the optimized structures are slightly distorted from ideal symmetries due to numerical noise arising from the grid. The values shown in the text are averages; however, the distortion is not larger than 0.01 Å for equivalent bond distances and 2° for equivalent angles.

The binding energies have been estimated with respect to singlet N_2 and the quintet ground state of the Fe atom. The importance of making explicit the atomic reference energy used to evaluate binding energies has been discussed[11,29] elsewhere. The calculation of Fe has been performed by relaxing all symmetry and configuration restrictions. The total energies of all calculated species are shown in Table 1. The Mulliken population analysis for the Fe atom gives a $d^{6.412}$ $s^{1.587}$ configuration. The basis set superposition error (BSSE) in the metal−ligand binding energies is expected to be the largest for $Fe(N_2)_5$, since it has the most ligands around the metal center. We have estimated the BSSE for $Fe(N_2)_5$ at about 0.7 kcal mol^{-1} with respect to complete dissociation which is sufficiently small for our purposes. Hence, the binding energies have not been corrected for BSSE.

For the most stable species, vibrational analyses were performed and their isotopically substituted species were analyzed by the harmonic approach. The Hessian matrix was evaluated numerically from the analytical gradients of the potential energy surface.

Table 1. Calculated Total Energies of the End-On $Fe(N_2)_n$ Complexes

complex	$2S_Z+1$	tot. energy (au)	rel energy (kcal mol^{-1})
FeN_2	1	−1373.212 11	15.1
	3	−1373.232 58	2.4
	5	−1373.236 35	0.00
$Fe(N_2)_2$	1	−1482.840 96	11.6
	3	−1482.860 30	0.0[a]
$Fe(N_2)_3$	1	−1592.441 69	18.4
	3	−1592.471 08	0.0
$Fe(N_2)_4$	1	−1702.057 64	4.1
	3	−1702.064 26	0.0
$Fe(N_2)_5$	1	−1811.647 69	0.0
N_2	1	−109.565 83	
Fe[b]	5	−1263.656 55	

[a] An optimized side-on $Fe(N_2)_2$ complex is 1.2 kcal mol^{-1} more stable. See text for details. [b] The Mulliken population analysis gives a $d^{6.412}$ $s^{1.587}$ configuration. See text for details.

Table 2. Dissociation Energies ($\bar{D}_e$ and D_e, kcal mol^{-1}) and Geometrical Properties (Å) of the End-On $Fe(N_2)_n$ Complexes

complex	Fe−N	N−N	$\bar{D}_e$[a]	D_e[b]
N_2		1.112		
FeN_2[c]	1.865 (1.711)	1.143 (1.148)	8.8	8.8
$Fe(N_2)_2$	1.789	1.135	22.6	36.5
$Fe(N_2)_3$[d]	1.828 (1.836)	1.136 (1.137)	24.5	28.2
$Fe(N_2)_4$[e]	1.864 (1.872)	1.130 (1.129)	22.6	17.2
$Fe(N_2)_5$[f]	1.860 (1.842)	1.130 (1.126)	20.3	11.0

[a] Mean binding energy calculated from the energy necessary to dissociate the complex into metal and ligands divided by the number of ligands. [b] Energy necessary to dissociate one ligand from the complex. [c] Values within parentheses correspond to the triplet state. [d] Values within parentheses correspond to the *z*-axis ligand. [e] Values within parentheses correspond to the other nonequivalent atoms of the C_{2v} structure. See text for details. [f] Values within parentheses correspond to the axial ligands.

Results and Discussion

We discuss first the complexes with end-on bonding. Complexes with side-on bonding are considered later.

A. Electronic Structure of End-On $Fe(N_2)_n$ Complexes. Table 1 shows the total energy of all complexes for various multiplicities as well as the relative energies. The complexes with $2S_Z + 1 = 5$ are at least 15.0 kcal mol^{-1} higher in energy than the ground state, with the exception of FeN_2, which has a quintet ground state. Two different (but useful) definitions of binding energies are being used in our discussion: D_e is the energy necessary to dissociate one ligand from the complex, and $\bar{D}_e$ is the mean binding energy calculated from the energy necessary to dissociate the complex into metal and ligands divided by the number of ligands. Table 2 shows the geometrical properties and the binding energies (D_e and $\bar{D}_e$) of the ground state of each complex.

It has been shown that a diatomic molecule interaction with a metal center can be rationalized and qualitatively predicted from a molecular orbital picture.[30] N_2 is isoelectronic with CO. The 5σ MO of CO is mostly localized on the carbon atom, while in N_2 the corresponding orbital $3\sigma_g$ (hereafter called 5σ in analogy with CO) is delocalized over the two nitrogen centers. According to Blanchet et al.,[30] the d_σ and 4s orbitals of the metal center and 5σ orbital of the diatomic molecule interact to yield three σ MOs: bonding (σ_b), nonbonding (σ_{nb}), and antibonding (σ_{ab}). The d orbitals with δ symmetry remain as nonbonding orbitals, and the d_π orbitals interact with the π^* orbitals of the

(18) St-Amant, A.; Salahub, D. R. *Chem. Phys. Lett.* **1990**, *169*, 387.
(19) Casida, M. E.; Daul, C. D.; Goursot, A.; Koester, A.; Petterson, L.; Proynov, E.; St-Amant, A.; Salahub, D. R. (principal authors); Duarte, H. A.; Godbout, N.; Guan, J.; Jamorski, C.; Leboeuf, M.; Malkin, V.; Malkina, O.; Sim, F.; Vela, A. (contributing authors). deMon Software-deMon-KS3 Module. University of Montreal, 1996.
(20) Becke, A. D. *Phys. Rev. A* **1988**, *38*, 3098.
(21) Perdew, J. P. *Phys. Rev. B* **1986**, *34*, 7406E.
(22) Perdew, J. P. *Phys. Rev. B* **1986**, *33*, 8822.
(23) Perdew, J. P. *Physica B* **1991**, *172*, 1.
(24) Perdew, J. P.; Chevary, J. A.; Vosko, S. H.; Jackson, K. A.; Pederson, M. R.; Singh, D. J.; Fiollhais, C. *Phys. Rev. B* **1992**, *46*, 6671.
(25) Perdew, J. P.; Wang, Y. *Phys. Rev. B* **1986**, *33*, 8800.
(26) Godbout, N.; Salahub, D. R.; Andzelm, J.; Wimmer, E. *Can. J. Chem.* **1992**, *70*, 560.
(27) Godbout, N. Thèse de doctorat, Université de Montréal, 1996.
(28) See: Schlegel, H. B. In *Ab-Initio Methods in Quantum Chemistry-I*; Lawley, K. P., Ed.; Wiley: New York, 1987.
(29) Baerends, E. J.; Branchadell, V.; Sodupe, M. *Chem. Phys. Lett.* **1997**, *265*, 481. Becke, A. D.; Savin, A.; Stoll, H. *Theor. Chim. Acta* **1995**, *91*, 147. Jones, R. O.; Gunnarsson, O. *Rev. Mod. Phys.* **1989**, *61*, 689. Russo, T. V.; Martin, R. L.; Hay, P. J. *J. Chem. Phys.* **1994**, *101*, 7729. Daul, C. *Int. J. Quantum Chem.* **1994**, *52*, 867. Ziegler, T.; Rauk, A.; Baerends, E. J. *Theor. Chim. Acta* **1977**, *43*, 261.
(30) Blanchet, C.; Duarte, H. A.; Salahub, D. R. *J. Chem. Phys.* **1997**, *106*, 8778.

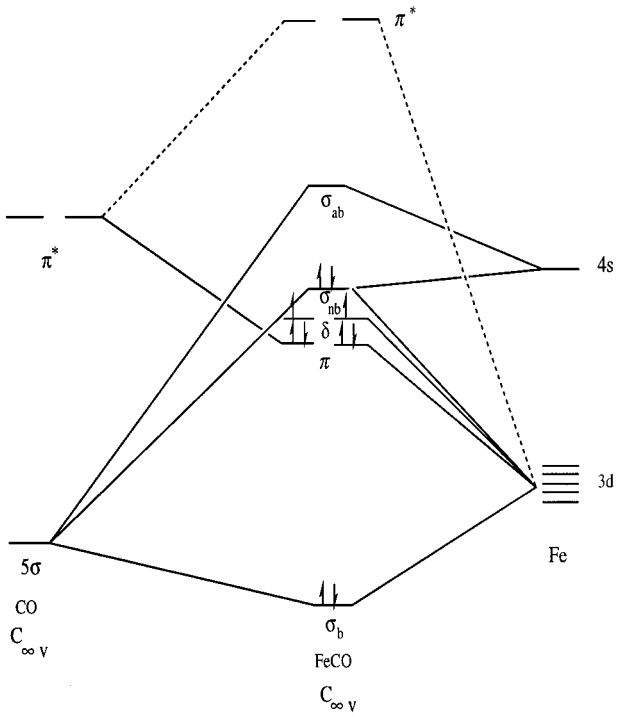

Figure 1. Correlation diagram for the triplet FeCO molecule. Only the most important orbitals to describe the Fe−CO bond are shown.

diatomic molecule. The σ_{nb} and the δ MOs are close in energy, favoring high-spin multiplicities due to the exchange energy. Particularly for FeCO, the δ and σ_{nb} orbitals account for 4 electrons favoring the triplet state (see Figure 1). The LUMO (lowest unoccupied molecular orbital), σ_{ab}, lies at higher energy because of the 5σ repulsion represented by the pair of electrons on the carbon atom. The σ_{ab} orbital is responsible for the bending of the species with high multiplicities because it can stabilize by breaking the symmetry. Fournier[11] predicted that the ground state of FeCO is a triplet and the quintet state lies 4.1 kcal mol^{-1} higher in energy with an Fe−C−O angle of about 158°. The isoelectronic species FeN_2 is expected to be different because N_2 is an apolar molecule and the 5σ MO is delocalized over both nitrogen centers. Therefore, the σ_{ab} orbital (see Figure 1) is expected to have lower energy in FeN_2; hence the triplet and quintet states should be close in energy. One could say that the 5σ repulsion is not as strong in FeN_2 as it is in FeCO. Hence, the quintet state might be linear or only slightly bent.

Triplet FeN_2 lies 2.4 kcal mol^{-1} higher in energy than the quintet ground state. However, using the GGA-PP[21,22,25] scheme, the ground state is predicted to be the triplet and the quintet state lies 0.6 kcal mol^{-1} higher in energy. Actually, the predicted ground state depends strongly on the exchange and correlation functional used, as shown in Table 3. The discrepancies between GGA-BP and GGA-PP schemes are due to the differences in describing the exchange energy. In fact, the triplet−quintet gap in FeN_2 is in the usual range of error of the GGA exchange functional used. We have also calculated this molecule using the XC functional scheme GGA-PW91.[23,24] The quintet is predicted to be the ground state, and the triplet lies only 0.2 kcal mol^{-1} higher in energy. Hence, one cannot decide the ground state solely on the basis of the calculated relative energies. One could ask whether the spin contamination associated with the KS wave function is affecting this result. The calculated values of $S(S+1)$ in Table 3 show that this is not the case; the spin contamination is rather small and can be neglected. The π back-donation from the occupied d orbitals

Table 3. Properties of End-On FeN_2 Calculated by Using Different XC Functionals

	GGA-BP[a]		GGA-PP[b]		GGA-PW91[c]	
$2S+1$	3	5	3	5	3	5
energy[d]	2.4	0.0	0.0	0.6	0.2	0.0
$S(S+1)$	2.18	6.19	2.16	6.18	2.09	6.23
Fe−N1 (Å)	1.711	1.866	1.723	1.895	1.684	1.830
N1−N2 (−)	1.148	1.142	1.146	1.142	1.148	1.146

[a] GGA-BP uses the exchange due to Becke[20] and correlation due to Perdew.[21,22] [b] GGA-PP uses the exchange due to Perdew and Wang[25] and the correlation due to Perdew[21,22] [c] GGA-PW91 uses the exchange due to Perdew[23] and the correlation due to Perdew et al.[24] [d] Energy difference in kcal mol^{-1}.

of the iron to the unoccupied π^* orbital of N_2 contributes to the increase of the N−N bond length by about 0.03 Å. The charge distribution on FeN_2 also shows a transfer of electrons from the metal center to the N_2 (see Table 4) of about 0.22 electron. In terms of the molecular orbital diagram shown in Figure 1, the quintet has a singly occupied σ_{ab} orbital that has contributions from the atomic orbitals (AOs) of the three centers. On the other hand, the triplet state has σ_{ab} unoccupied and σ_{nb} is doubly occupied. This orbital is a nonbonding orbital centered on the metal, so it does not contribute to the charge transfer, explaining why the triplet state shows a smaller charge on the iron atom with respect to the quintet state. Most of the charge observed on the triplet FeN_2 is then due to the π back-donation via Fe d_π and N_2 π^* orbital interactions. The difference in Fe−N bond distance between quintet and triplet states of 0.15 Å is also consistent with removing an antibonding electron.

Recently, Castro et al.[15] reported a density functional study of the $Fe-N_2$ complex. According to them, the triplet end-on-bound $Fe-N_2$ is the ground state (in agreement with our GGA-PP results, Table 3), and the side-on geometry is at 2.1 kcal mol^{-1} using GGA-PP.[21,22,25] They found the quintet state 13.0 kcal mol^{-1} above the triplet ground state. Our GGA-PP (Table 3) results give a nearly degenerate state with the quintet lying only 0.6 kcal mol^{-1} higher in energy than the ground state, which is very different from their result. Their predicted Fe−N and N−N bond lengths are 1.71 and 1.16 Å, respectively, and may be compared to our calculated values of 1.711 and 1.148 Å for the respective triplet state. Our calculated binding energy is in good agreement with their predicted value of 8.76 kcal mol^{-1}.

The triplet $Fe(N_2)_2$ is the predicted ground state. Due to the fact that the complex is linear, the trans effect is observed in the binding energy, $\bar{D}_e$, which is 13.8 kcal mol^{-1} larger in comparison to that of FeN_2. The energy necessary to dissociate one ligand from $Fe(N_2)_2$, D_e, is 36.5 kcal mol^{-1}, while for the case of FeN_2 it is only 8.8 kcal mol^{-1}. This large increase of the binding energy can be rationalized if one notes that when an N_2 is added to FeN_2, the 5σ and π^* orbitals of the incoming N_2 will interact with the FeN_2 MOs in the same way as for the case of FeN_2. The two 5σ orbitals of the N_2 ligands and the d_σ orbital of the Fe result in four σ MOs, two of which are bonding and doubly occupied, contributing to the increase of the binding energy. The charge on the metal center is larger when compared to the case of triplet FeN_2, showing that the π back-donation interaction in $Fe(N_2)_2$ is more effective than that in FeN_2. The N−N bond distance is 0.025 Å larger than that for free N_2, and the Fe−N bond distance is 1.789 Å, 0.078 Å larger than the value for triplet FeN_2.

The optimization of the $Fe(N_2)_3$ complex was started using a D_{3h} geometry with the three N_2 molecules in the plane; however, a Jahn−Teller distortion reduced the symmetry to close to C_{2v}

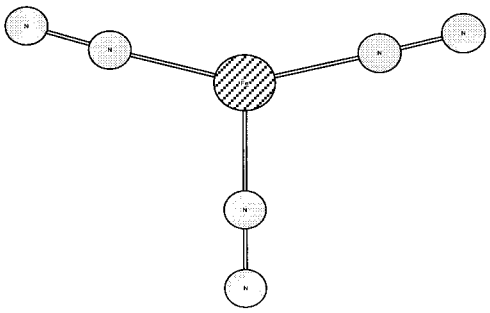

Figure 2. Optimized geometry of $Fe(N_2)_3$. It has a distorted C_{2v} geometry.

(Figure 2). Barnes et al.[12] have optimized $Fe(CO)_3$ with the constraint of C_{3v} symmetry. They found the triplet the most stable. Following them, we have also optimized $Fe(N_2)_3$ starting with a C_{3v} structure; however, the optimization has been performed without symmetry constraints. We found a minimum with C_{3v} geometry about 6.0 kcal mol^{-1} higher in energy than that of the C_{2v} species. The triplet state shows the lowest energy followed by the singlet, 18.4 kcal mol^{-1} higher in energy. The Fe−N bond distance along the *z* axis according to the principal rotation axis of the C_{2v} group is 0.01 Å longer than the other Fe−N bond distances. The other two ligands make an angle of 150°, forming almost a **T** geometry. $Fe(N_2)_3$ is formed from the interaction of the linear $Fe(N_2)_2$ (axial) with another N_2 molecule (equatorial) in such a way that the $Fe(N_2)_2$ moiety is distorted from its original linear structure by about 30°, hence diminishing the trans effect. Consequently, the axial Fe−N bonds become weaker, but they are still stronger than the equatorial Fe−N bond. The D_e of 28.2 kcal mol^{-1} may be assigned to the equatorial Fe−N_2 dissociation. The Fe atom in $Fe(N_2)_3$ presents the largest charge with respect to those of the other studied complexes, showing that the π back-donation is important in this complex.

The tetrahedral $Fe(N_2)_4$ complex converged to the geometry shown in Figure 3 with a distorted C_{2v} symmetry. The triplet is the ground state and the singlet, with a distorted D_{2d} symmetry, lies 4.1 kcal mol^{-1} above. We have also optimized the planar complex; however, it is a transition state since it has a normal mode with an imaginary frequency. The $\bar{D}_e$ is smaller, showing that the interaction between each ligand and the metal site is smaller. The energy necessary to dissociate one ligand is just 17.2 kcal mol^{-1}, almost half of the value observed for $Fe(N_2)_3$. The net charge on the metal is smaller, which is expected because the metal is quite saturated. Moreover, the transfer of electrons from the metal to the ligands via back-donation is not favored, since the number of electrons available at the metal center to be back-donated to each ligand is smaller.

Ziegler et al.[10] have calculated the dissociation energies of $Fe(CO)_5$ using a DFT method. $Fe(CO)_4$ was predicted to be D_{2d} with $\lambda = \tau = 162°$ (see Figure 4). Barnes et al. have also calculated $Fe(CO)_4$ using the modified coupled-pair functional (MCPF) method. They have predicted a C_{2v} symmetry with $\lambda = 150°$ and $\tau = 104°$. The experimental values, estimated from ultraviolet spectra of $Fe(CO)_4$ in an SF_6 matrix,[8] are 145 and 120° for λ and τ, respectively, and indicate that the complex belongs to the C_{2v} symmetry group. The isoelectronic species $Fe(N_2)_4$ is predicted to be a C_{2v} triplet with $\lambda = 139°$ and $\tau = 101°$. The singlet state lies 4.1 kcal mol^{-1} higher in energy and is predicted to be D_{2d} with $\lambda = \tau = 150°$, relatively close to the estimated values for $Fe(CO)_4$. The angle of 150° is equal to the angle between the axial ligands in $Fe(N_2)_3$; hence the trans effect is present to some extent in the singlet state of $Fe(N_2)_4$. Tetracarbonyliron is predicted to have a triplet ground state[12] with the singlet lying 19 kcal mol^{-1} higher. Actually, there is experimental evidence that $Fe(CO)_4$ is paramagnetic.[9] The ground state of $Fe(N_2)_4$ is also predicted to be a triplet with the singlet state lying only 4.1 kcal mol^{-1} higher in energy.

Figure 5 shows the optimized geometry of $Fe(N_2)_5$. It is a trigonal-bipyramidal-like $Fe(CO)_5$. The N−N bond distance in $Fe(N_2)_5$ is 0.018 Å longer than that in the calculated free N_2 molecule, providing evidence for weaker back-donation with respect to that of the unsaturated complexes. The $Fe(N_2)_5$ complex has axial Fe−N bond distances 0.035 Å smaller than the equatorial Fe−N distances. In contrast, its isoelectronic species $Fe(CO)_5$ has longer axial distances.[12] The $\bar{D}_e$ of $Fe(N_2)_5$ is 2.3 kcal mol^{-1} smaller than that for the $Fe(N_2)_4$ species, following the same trend observed for the other complexes. The dissociation energy, D_e, however, is 6.2 kcal mol^{-1} smaller than that for $Fe(N_2)_4$, showing that the destabilizing N_2/N_2 steric repulsions in the highly symmetric D_{3h} $Fe(N_2)_5$ predominate in relation to the stabilizing N_2−Fe interactions.

Table 4 shows the net charge on each nonequivalent atom. The charge on the Fe atom increases nonlinearly when an N_2 molecule is added because the number of electrons available on the Fe to back-donate to each ligand is smaller. When five N_2 ligands are placed around the Fe atom, the electron transfer from the metal to each ligand via π back-donation is not efficient, so the charge on the Fe is drastically decreased.

Figures 6 and 7 show contour maps of two MOs involving axial and equatorial ligands where the σ donation interaction is well characterized. The MOs that describe the σ donation are distributed over the whole molecule as is expected, since the 5σ MO of N_2 is completely delocalized. Figures 8 and 9 show two MOs that characterize the π back-donation involving axial and equatorial N_2 molecules.

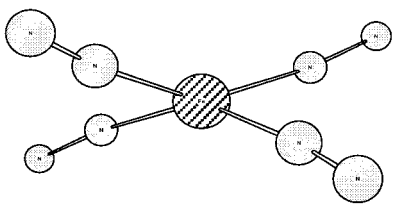

singlet D_{2d}

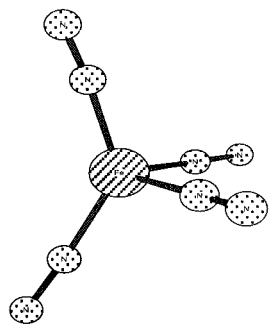

triplet C_{2v}

Figure 3. Optimized geometries of $Fe(N_2)_4$.

Table 4. Mulliken Population Analysis of the $Fe(N_2)_n$ Complexes

	net charge[a]			bond order	
complex	Fe	N1	N2	Fe−N1	N1−N2
FeN_2[b]	0.22 (0.15)	−0.19 (−0.08)	−0.03 (−0.07)	0.888 (0.973)	2.517 (2.445)
$Fe(N_2)_2$	0.18	−0.08	−0.01	0.765	2.544
$Fe(N_2)_3$[c]	0.29	−0.08 (−0.07)	−0.01 (−0.03)	0.737 (0.773)	2.581 (2.581)
$Fe(N_2)_4$[d]	0.14	−0.02 (−0.02)	−0.01 (−0.02)	0.683 (0.712)	2.618 (2.635)
$Fe(N_2)_5$[e]	0.03	0.01 (0.00)	−0.02 (−0.01)	0.695 (0.707)	2.637 (2.642)

[a] N1 are the nearest neighbor of the Fe atoms. N2 are the atoms bonded to the N1 atoms. [b] Values within parentheses correspond to the triplet state. [c] Values within parentheses correspond to the *z*-axis ligand. [d] Values within parentheses correspond to the other nonequivalent atoms of the C_{2v} structure. See text for details. [e] Values within parentheses correspond to the axial ligands.

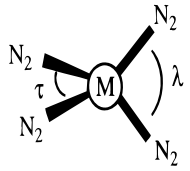

Figure 4. Definition of λ and τ angles in an ML_4 complex.

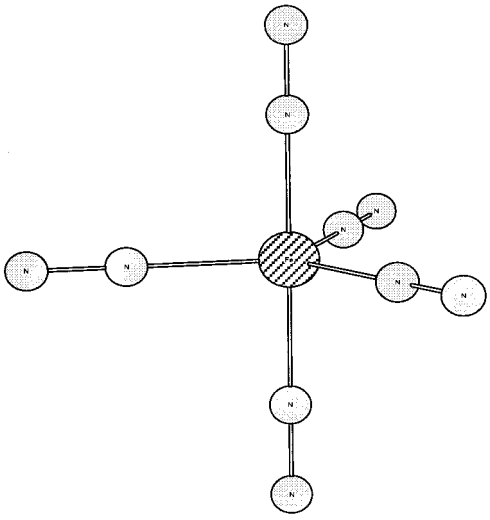

Figure 5. Optimized geometry of $Fe(N_2)_5$. It has a (slightly distorted) D_{3h} geometry.

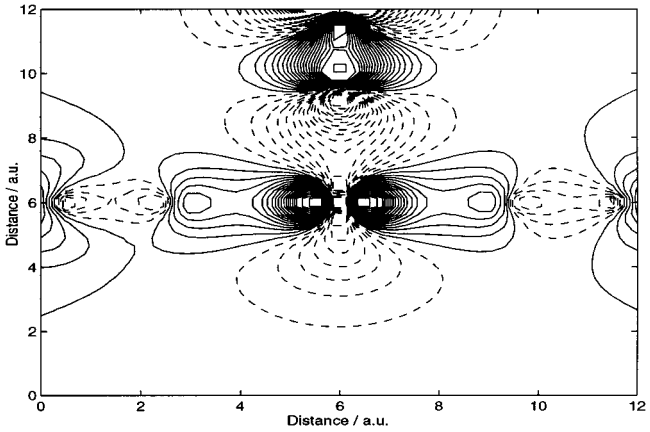

Figure 6. Contour map of an $Fe(N_2)_5$ molecular orbital. It corresponds to the σ donation of the axial N_2 molecules to the Fe atom.

From Tables 2 and 4 we observe the trends when N_2 ligands are added to an Fe atom until it is saturated with a coordination number (CN) equal to 5. If we take the change of the N−N bond length as a measure of the π back-donation, we observe that it diminishes from CN = 1 to CN = 5. $Fe(N_2)_2$ has the largest dissociation energy, D_e, followed by $Fe(N_2)_3$. The trans effect favors σ donation and π back-donation interactions.

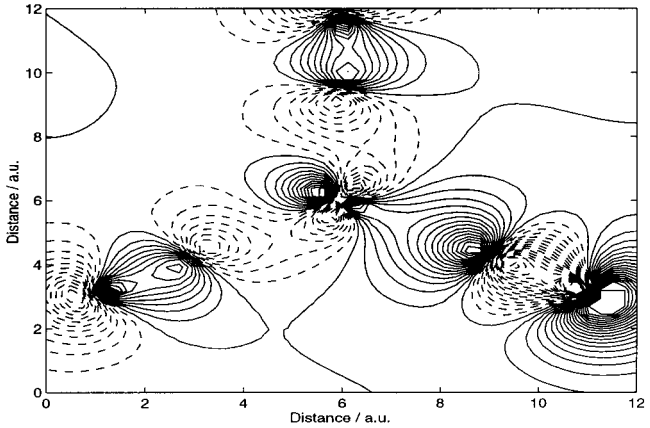

Figure 7. Contour map of an $Fe(N_2)_5$ molecular orbital. It corresponds to the σ donation of the equatorial N_2 molecules to the Fe atom.

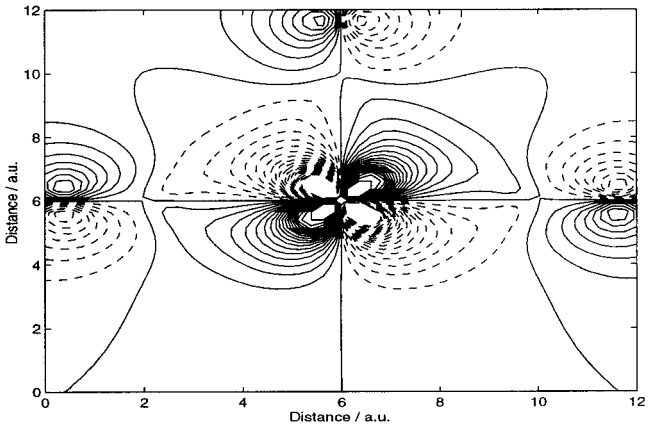

Figure 8. Contour map of an $Fe(N_2)_5$ molecular orbital. It corresponds to the back-donation from the Fe atom to the axial N_2 molecules.

Increasing CN to 4 or 5 decreases the D_e rapidly. The mean dissociation energy, D_e, follows the same trends as the dissociation energy, D_e. The Mulliken population analysis also shows the trends along this series of complexes. The charge on the metal center can be taken as a measure of the π back-donation. It decreases when one increases the CN. It is interesting to observe that the saturated species (CN = 5) presents the largest decrease of the charge on the iron atom. One could explain this by realizing that, on an increase in the CN, the availability of electrons to be back-donated from the iron to each π^* N_2 orbital is diminished because all ligands are competing for electrons. The bond orders follow the same trends; however, as the difference is small, one should not take this as definitive. Nevertheless, if they are compared to the typical values observed for Fe−CO bonds (about 1.0), the orders of Fe−N_2 bonds indicate that they are weaker but, however, stronger than van der Waals interactions.

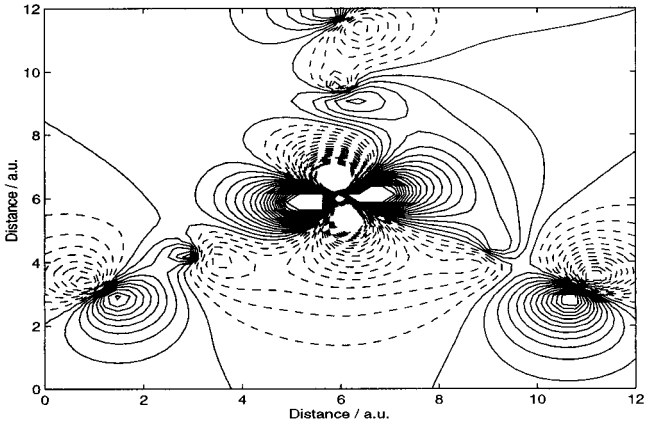

Figure 9. Contour map of an $Fe(N_2)_5$ molecular orbital. It corresponds to the back-donation from the Fe atom to the equatorial N_2 molecules.

Table 5. Calculated Properties of the $Fe(CO)_5$ and $Fe(N_2)_5$ Complexes

property[b]	$Fe(N_2)_5$	$Fe(CO)_5$
	Bond Lengths[a] (Å)	
Fe−LG	1.860 (1.842)	1.803 (1.804)
L−G	1.1300 (1.126)	1.162 (1.159)
free L−G	1.112	1.145
	Mean Binding Energies (kcal mol^{-1})	
Fe−LG	20.3	42.8
	Net Charges[a]	
Fe	0.03	−0.50
L	0.01 (0.00)	0.35 (0.29)
G	−0.02 (−0.01)	−0.23 (−0.22)
	Bond Orders[a]	
Fe−L	0.695 (0.707)	1.074 (1.015)
L−G	2.637 (2.642)	2.244 (2.255)

[a] Values within parentheses correspond to the axial ligands. [b] LG is the ligand. L can be carbon or nitrogen, and G, oxygen or nitrogen.

The isoelectronic molecule $Fe(CO)_5$ has been intensively studied (see refs 10, 12, 31, and 32 and references therein). We have calculated $Fe(CO)_5$ using the same quality of basis sets as for the N_2 complexes. The results are shown in Table 5 together with the results for $Fe(N_2)_5$. The 5σ MOs of CO are more localized on the carbon atom, making the interaction of CO with Fe stronger due to a more efficient σ donation, resulting in a net charge on the Fe of −0.5 au. On the other hand, the net charge on the Fe atom in the $Fe(N_2)_5$ complex is only 0.03 au. $Fe(CO)_5$ presents more separation of charge, while in $Fe(N_2)_5$, the separation of charges does not exceed 0.05 au. The Fe−C bond distances are 0.06 Å smaller than the Fe−N bond distances, as is expected. The mean binding energy is 42.8 kcal mol^{-1} for $Fe(CO)_5$, and it is about 22.5 kcal mol^{-1} larger than the mean binding energy of $Fe(N_2)_5$.

B. Vibrational Analysis of the End-On Complexes. Infrared spectra have been widely used to characterize atoms and molecules isolated in rare-gas matrixes (for example, see ref 33 and references therein). Barret and Montano reported on Fe and its dimer isolated in a solid nitrogen matrix using infrared and Mössbauer experiments. Recently, Haslett et al.[7] detected dinitrogen iron complexes in a nitrogen matrix using FTIR (Fourier transform infrared). We have performed a harmonic vibrational analysis of all complexes in their predicted ground states. Table 6 shows the harmonic frequencies and the infrared intensities of unsaturated complexes. The frequencies related to the symmetric N−N stretch increase with increasing coordination number. FeN_2 has a σ^+ frequency of 2048.0 cm^{-1}, which increases to 2178.8 cm^{-1} for $Fe(N_2)_4$. The opposite trend is observed for the Fe−N stretch, which increases up to $Fe(N_2)_3$, and for CN = 3 and 4 the symmetric Fe−N stretch is about 440 cm^{-1}. $Fe(N_2)_5$ has a smaller Fe−N stretch of about 400 cm^{-1}.

Table 7 compares the harmonic frequencies of $Fe(N_2)_5$ with the experimental and calculated values of its isoelectronic species $Fe(CO)_5$. The symmetry of the normal modes was assigned according to the D_{3h} group. It is expected that the frequencies with e′ symmetry are split because the optimized molecule is slightly distorted. Furthermore, the IR forbidden frequencies have some calculated intensities through mixing with IR allowed vibrations. This explains the IR intensity of 3.9 km mol^{-1} for an a_1' frequency of 2216.5 cm^{-1}. Moreover, the IR intensities are more sensitive to the distortion of the symmetry than the frequencies. The N−N frequency due to the completely symmetric motion was evaluated at 2216.5 cm^{-1}, which is about 140 cm^{-1} larger than the C−O frequency in $Fe(CO)_5$. The experimental N_2 and CO frequencies[34] are 2358.57 cm^{-1} and 2170 cm^{-1}, respectively. In the range 1900−2200 cm^{-1} of the spectra, the frequencies are related to the N−N or CO stretches and, consequently, $Fe(N_2)_5$ gives larger frequencies than $Fe(CO)_5$, as is expected. On the other hand, the Fe−N stretching frequencies are lower than those of the Fe−C stretches. The totally symmetric Fe−C frequency is about 80.0 cm^{-1} higher than the value for Fe−N stretches.

One could ask whether it would be possible to identify the $Fe(N_2)_5$ and $Fe(N_2)_4$ complexes in the nitrogen matrix experiments using FTIR. Therefore, we have studied the effect of the ^{15}N isotopic substitution on the vibrational frequencies of these two complexes in the 1900−2300 cm^{-1} range. This spectral range is easily accessible for most FTIR experiments. Tables 8−10 show the frequencies of the isotopically substituted $Fe(N_2)_5$ and $Fe(N_2)_4$ complexes, respectively. In Table 8, the symmetry of the normal modes is valid for the D_{3h} molecules. The frequencies of the partially isotopically substituted species have been assigned according to the similarity of their normal modes with those of the D_{3h} molecules. It is easier to follow the isotopic effect along the fully substituted species. The frequency a_2' is assigned to the N−N strength of the axial N_2 molecules, and it is invariant with respect to equatorial substitution; i.e., the frequency 2156.6 cm^{-1} is the same for the substitutions, namely *X*0 (which *X* means the number of equatorial $^{15}N_2$ molecules and 0 means the all axial molecules are $^{14}N_2$), and the frequency 2083.7 cm^{-1} is the same for *X*2 molecules. The e′ frequencies are assigned to the equatorial motions and are invariant with respect to the axial substitutions. The a_1' frequencies involve motions in all five N_2 ligands and therefore vary with all substitutions. The frequencies of the partially isotopically substituted $Fe(N_2)_4$ complex are shown in Tables 9 and 10 for the singlet and triplet states, respectively. The frequencies of the partially isotopically substituted molecules have been assigned to the D_{2d} or C_{2v} symmetry groups according to the similarity of their normal modes with those of

(31) Frenking, G.; Dapprich, S.; Ehlers, A. W.; Otto, M.; Vyboishchikov S. F. In *Metal-Ligand Interactions*; NATO ASI Series C474; Russo, N., Salahub, D. R., Eds.; Kluwer: Dordrecht, The Netherlands, 1996; pp 185−232.
(32) Daniel, C.; Bérnard, M.; Dedieu, A.; Wiest, R.; Veillard, A. *J. Phys. Chem.* **1984**, *88*, 4805.
(33) Braterman, P. S. *Metal Carbonyl Spectra*; Academic: London, 1975.
(34) Huber, K. P.; Herzberg, G. *Molecular Spectra and Molecular Structure. IV. Constants of Diatomic Molecules*; Van Nostrand Reinhold Co.: New York, 1979.
(35) Delley, B.; Wrinn, M.; Lüthi, H. P. *J. Chem. Phys.* **1994**, *100*, 5785.
(36) Lee, C.; Yang, W.; Parr, R. G. *Phys. Rev. B* **1988**, *37*, 785.

Table 6. Calculated Frequencies (cm^{-1}) of the End-On Unsaturated Complexes with Their Infrared Intensities (km mol^{-1}) in Parentheses

$C_{\infty v}$-FeN_2		$D_{\infty h}$-$Fe(N_2)_2$		C_{2v}-$Fe(N_2)_3$		$Fe(N_2)_4$[a] singlet D_{2d}		$Fe(N_2)_4$[a] triplet C_{2v}	
σ^+	2052.2 (234.6)	σ_g^+	2136.2 (0.0)	a_1	2139.1 (0.4)	a_1	2178.8 (0.1)	a_1	2178.5 (9.6)
	419.1 (0.9)		442.7 (0.0)		2062.2 (802.8)		439.8 (0.0)		2102.1 (460.0)
π	158.9 (2.2)	σ_u^+	2070.3 (5.3)		444.5 (32.3)		392.1 (1.4)		412.5 (22.1)
	156.0 (6.0)		546.1 (0.2)		443.8 (0.1)		390.1 (14.6)		399.3 (2.4)
		π_g	271.6 (0.0)		395.3 (2.3)		50.0 (0.0)		373.0 (10.4)
			250.7 (0.0)		69.5 (1.1)	a_2	292.3 (2.3)		353.3 (1.8)
		π_u	380.3 (1.6)	a_2	231.8 (0.0)	b_1	480.2 (0.0)		77.1 (0.9)
			347.3 (5.1)	b_1	399.1 (2.5)		95.9 (0.4)		54.9 (0.5)
			80.7 (0.1)		203.4 (0.6)	b_2	2096.2 (182.8)	a_2	345.2 (0.74)
			80.0 (0.1)		67.3 (3.0)		440.8 (0.04)		244.2 (0.3)
				b_2	2066.7 (42.2)		83.7 (3.4)		66.3 (0.1)
					502.5 (0.1)	e	2104.6 (170.0)	b_1	2109.0 (489.2)
					367.0 (3.2)		2101.4 (195.7)		404.6 (23.3)
					269.9 (1.6)		568.8 (0.63)		396.8 (4.3)
					77.2 (0.1)		567.9 (0.03)		236.9 (0.13)
							416.9 (0.4)		77.8 (0.6)
							416.8 (0.7)	b_2	2099.8 (459.9)
							293.8 (2.3)		460.7 (20.4)
							290.8 (5.8)		331.2 (4.6)
							98.9 (0.7)		238.3 (0.7)
							97.7 (0.4)		75.5 (0.3)

[a] The triplet $Fe(N_2)_4$ is the ground state, and the singlet lies 4.1 kcal mol^{-1} higher in energy.

Table 7. Comparison of the Published Frequencies of $Fe(CO)_5$ and the Calculated Frequencies of $Fe(N_2)_5$ (cm^{-1}) with Their Infrared Intensities (km mol^{-1}) in Parentheses[a]

	$Fe(CO)_5$ BLYP[c]	$Fe(CO)_5$ GGA-BP	$Fe(CO)_5$ exp[b]	$Fe(N_2)_5$		$Fe(CO)_5$ BLYP[c]	$Fe(CO)_5$ GGA-BP	$Fe(CO)_5$ exp[b]	$Fe(N_2)_5$
a_1'	2072	2095.3 (0.09)	2116	2216.5 (3.9)	a_2''	1989	2012.0 (0.05)	2002	2156.6 (6.3)
	1991	2014.6 (0.06)	2030	2135.1 (1.0)		610	634.0 (0.04)	615	502.1 (3.8)
	471	465.3 (0.0)	418	396.4 (0.0)		480	495.4 (0.03)	432	414.3 (3.5)
	419	435.6 (0.01)	381	372.8 (0.0)		105	104.1 (0.1)	72	102.7 (1.8)
a_2'	349	354.1 (0.2)	278	281.2 (4.4)	e''	539	552.1 (0.0)	491	449.6 (0.0)
e'	1974	1997.1 (0.68)	1979	2128.7 (40.2)			551.0 (0.0)		447.4 (0.0)
		1996.4 (0.86)		2126.1 (21.3)		363	370.8 (0.0)	448	273.0 (0.0)
	646	666.6 (0.30)	637	545.1 (10.6)			368.3 (0.0)		271.4 (0.1)
		665.8 (0.27)		543.0 (7.7)		94	93.8 (0.0)	132	95.7 (0.0)
	479	502.0 (0.1)	554	422.1 (1.0)			92.8 (0.0)		95.3 (0.0)
		501.5 (0.08)		421.3 (0.5)					
	424	443.5 (0.0)	475	342.6 (0.0)					
		436.2 (0.05)		340.6 (0.1)					
	103	100.5 (0.06)	112	109.2 (0.3)					
		99.84 (0.07)		108.3 (0.3)					
	54	53.1 (0.0)	64	52.4 (0.4)					
		50.5 (0.0)		49.0 (0.1)					

[a] The experimental N_2 and CO frequencies are 2358.57 and 2170.0 cm^{-1}, respectively.[34] [b] Reference 33. [c] The calculated values are from ref 35. The GGA BLYP scheme has the exchange functional proposed by Becke[20] and the correlation functional proposed by Lee, Yang, and Parr.[36]

D_{2d} and C_{2v} molecules depending on whether the molecules are singlet or triplet, respectively. It is important to observe that the infrared (IR) active frequencies of $Fe(N_2)_4$ are in the same range of frequencies as those of $Fe(N_2)_5$. $Fe(N_2)_4$ has the b_2 frequencies 2096.2 cm^{-1} and two nearly degenerate 2104.6 and 2101.4 cm^{-1} IR-active modes, while the saturated species, $Fe(N_2)_5$, has also 2156.6 cm^{-1} and two nearly degenerate 2128.7 and 2126.1 cm^{-1} IR-active modes. The mean error assigned to the calculated harmonic frequencies is expected to be about 50 cm^{-1}. Hence, one would expect that these two complexes would have IR spectra with the same shapes. If the complexes do not have distortions from their symmetries, the two spectra would be similar, at least, in this range of the spectra. Unfortunately, the Raman spectra of these two complexes are also similar and would not help to distinguish them in the nitrogen matrix.

According to our results, the three peaks observed by Haslett et al.[7] are due to the end-on species. The small peaks around 1900 cm^{-1} could be an indication that side-on species are present in small quantities; however these species are at least 11.5 kcal mol^{-1} higher in energy.

C. Searching for Other Low-Lying Structures. The end-on $Fe(N_2)_n$ complexes compare well with their isoelectronic species $Fe(CO)_n$. In fact, the metal−ligand interaction mechanism for the end-on Fe−N_2 and Fe−CO complexes are similar. But the same is not true for the side-on complexes. The different ways that one or more N_2 ligands can interact with the metal center lead to a potential energy surface with several minima close in energy and difficult to analyze. In other words, the potential energy surfaces of these species are much more complex. We have explored extensively the potential energy surface searching for different structures. Of course, we cannot affirm that all possibilities have been tested but we believe that the most important ones have been calculated. We observed that, with the exception of the complex with coordination number (CN) 2, the end-on complexes are the most stable species.

Table 8. Calculated Frequencies (cm^{-1}) of Isotopically Substituted $Fe(^{15}N_2)_{x+y}(^{14}N_2)_{(3-x)+(2-y)}$ Molecules with Their Infrared Intensities (km mol^{-1}) in Parentheses

XY^a	a_2'	e′		a_1'	a'_1
00	2156.6(6.3)	2128.7(40.2)	2126.1(21.3)	2216.5(3.9)	2135.1(1.0)
01	2085.8(4.2)	2129.0(37.9)	2126.2(20.3)	2205.7(5.0)	2143.1(5.1)
02	2083.6(5.9)	2129.0(36.8)	2126.2(20.0)	2187.9(7.2)	2089.7(2.5)
10	2156.6(6.4)	2126.2(19.1)	2064.9(15.3)	2210.5(7.2)	2132.3(24.2)
11	2089.6(12.8)	2126.3(18.9)	2062.3(11.3)	2198.8(9.6)	2140.2(19.2)
12	2083.6(6.0)	2126.3(18.9)	2060.8(9.6)	2177.3(19.4)	2095.9(17.7)
20	2156.6(6.4)	2071.4(5.8)	2056.7(31.3)	2204.4(4.2)	2129.0(22.6)
21	2096.0(9.8)	2135.4(19.2)	2056.6(31.7)	2192.1(5.9)	2064.7(3.4)
22	2083.7(5.9)	2062.0(2.4)	2056.5(32.0)	2164.3(15.2)	2105.0(14.3)
30	2156.6(6.4)	2056.9(35.7)	2054.3(19.5)	2198.3(1.2)	2079.8(5.9)
31	2109.4(6.7)	2056.9(36.7)	2054.2(19.5)	2185.4(2.4)	2066.7(2.8)
32	2083.7(6.0)	2056.8(37.5)	2054.2(19.5)	2141.6(3.6)	2062.9(0.9)

[a] *X* is the number of equatorial and *Y* the number of axial $^{15}N_2$ molecules. The symmetry assignment is valid only for the D_{3h} molecules (*XY* = 00, 02, 30, 32). The other frequencies have been assigned in correspondence to the D_{3h} molecules.

Table 9. Calculated Frequencies of Isotopically Substituted Singlet $Fe(^{14}N_2)_{4-x}(^{15}N_2)_x$ Molecules (cm^{-1}) with Their Infrared Intensities (km mol^{-1}) in Parentheses

X^a	a_1	e		b_2
0	2178.8 (0.1)	2104.6 (170.0)	2101.4 (195.7)	2096.2 (182.8)
1	2168.1 (11.2)	2101.7 (210.0)	2098.9 (155.3)	2041.7 (163.2)
2S[b]	2156.8 (1.9)	2053.4 (11.7)	2100.0 (275.7)	2028.7 (241.3)
2T[b]	2154.9 (23.7)	2101.6 (181.7)	2033.7 (169.3)	2048.6 (155.9)
3	2140.2 (43.1)	2066.3 (133.0)	2033.7 (185.7)	2026.8 (160.0)
4	2105.4 (0.1)	2033.7 (158.8)	2030.6 (182.8)	2025.7 (170.7)

[a] X is the number of isotopically substituted N_2 molecules. The symmetry assignment is valid only for the D_{2d} molecules (*X* = 0, 4). The other frequencies have been assigned in correspondence to the D_{2d} molecules. [b] S or T mean that the two substitutions are in cis or trans position with respect to each other.

Table 10. Calculated Frequencies of Isotopically Substituted Triplet $Fe(^{14}N_2)_{4-x}(^{15}N_2)_x$ Molecules (cm^{-1}) with Their Infrared Intensities (km mol^{-1}) in Parentheses

X^a	a_1		b_1	b_2
0	2178.5 (0.1)	2102.1 (5.5)	2109.0 (4.9)	2099.8 (4.6)
1A	2167.2 (0.4)	2046.2 (4.9)	2104.5 (4.6)	2100.8 (4.9)
1B	2170.8 (0.6)	2102.4 (5.6)	2109.3 (4.7)	2036.6 (3.9)
2A	2151.2 (0.6)	2056.5 (5.7)	2101.1 (3.5)	2038.0 (4.6)
2B	2161.3 (1.3)	2047.0 (5.1)	2109.3 (5.0)	2030.0 (3.3)
2AB	2157.8 (1.4)	2030.4 (3.2)	2054.9 (6.7)	2104.2 (3.3)
3A	2136.2 (0.8)	2031.4 (5.3)	2038.0 (4.4)	2069.6 (3.9)
3B	2145.1 (1.7)	2033.0 (4.5)	2067.9 (3.7)	2029.7 (4.5)
4	2105.2 (0.1)	2031.4 (5.1)	2038.0 (4.6)	2029.1 (4.3)

[a] *X* is the number of isotopically substituted N_2 molecules. The symmetry assignment is valid only for the C_{2v} molecules (*X* = 0, 2A, 2B, 4). The other frequencies have been assigned in correspondence to the C_{2v} molecules. The labels A and B refer to the two N_2 molecules that are equivalent, A for the equivalent molecules with angle $\lambda = 139°$ and B with angle $\tau = 101°$. Label 2AB means that the two substitutions have been made, one for each pair of equivalent molecules.

Now, we turn to the discussion of the low-lying species.

The side-on FeN_2 complex has been calculated. The triplet is 2.4 kcal mol^{-1} higher in energy than that of the quintet end-on species. This is in agreement with previous reported results.[15,16] Castro et al.[15] have calculated the FeN_2 complex using GGA-PP, and according to them, the side-on geometry is 2.1 kcal mol^{-1} higher in energy than the triplet end-on complex. Neurock et al. have also calculated these species using GGA-BP, and they found that side-on geometry is 4.0 kcal mol^{-1} higher in energy than that of the triplet end-on species. The differences between the published GGA-BP and our results are due to the different basis sets used. We have used TZVP basis sets while Neurock et al.[16] used DZVP. The optimized geometry is in good agreement with the published results. The differences are not larger than 0.003 Å. The Fe−N bond length is predicted to be 1.860 Å and N−N is 1.199 Å. In comparison to those of the triplet end-on species, the Fe−N and N−N distances are 0.149 and 0.051 Å shorter than those of the side-on species. The net charge on the metal center in the side-on complex is 0.33 electron, showing that the N_2 σ donation is not favored in comparison to the end-on geometry, which has a smaller net charge on the Fe (about 0.22 electron). Furthermore, a transfer of charge density from the metal to the ligand through back-donation is favored because the side-on geometry enhances the interaction of the π^* orbitals of N_2 with the d orbitals of the metal atom. Consequently, the N−N frequency of side-on $Fe-N_2$ is about 350 cm^{-1} less than those of the end-on species, since the charge density transfer to the N_2 π^* orbitals weakens the N−N bond.

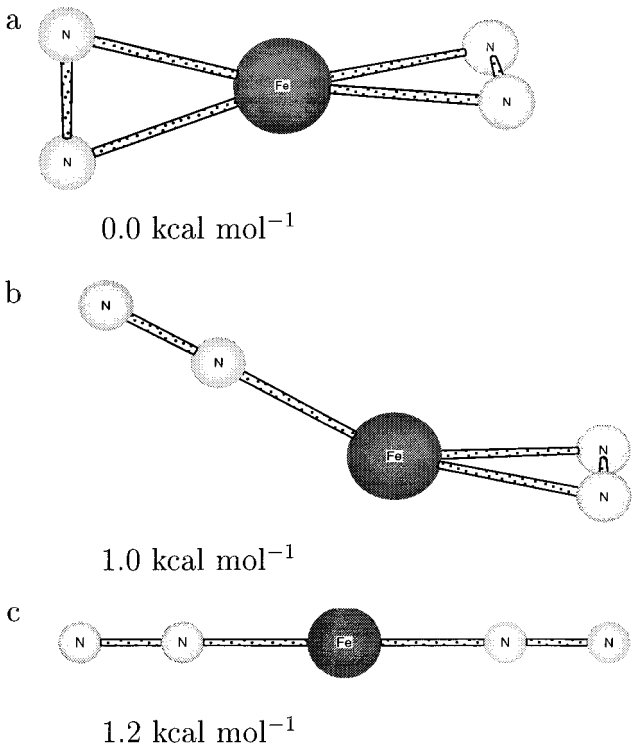

Figure 10. Relative energies of the optimized $Fe(N_2)_2$ geometries. They have triplet states.

Different $Fe(N_2)_2$ structures have been optimized. Three low-lying species are shown in Figure 10. Other species are at least 11.0 kcal mol^{-1} higher in energy. It is very difficult to predict which species shown in Figure 10 is, in fact, the most stable. As we have shown above for the case of end-on FeN_2, different

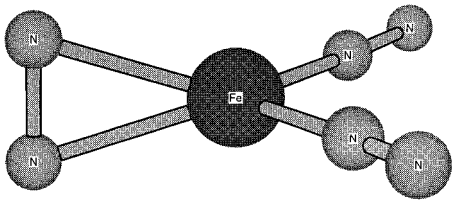

Figure 11. Optimized geometry of $Fe(N_2)_3$ with side-on N_2 bonding. It is a distorted C_{2v} symmetry.

XC functionals could change the relative stability of the species. The "a" species (Figure 10) has Fe−N and N−N bond distances predicted to be 1.905 and 1.185 Å; the "c" species has 1.789 and 1.136 Å, respectively. The "b" species has different Fe−N and N−N bond distances. The end-on ligand has 1.799 and 1.141 Å while the side-on N_2 has 1.913 and 1.183 Å for the Fe−N and N−N distances, respectively. The Mulliken population analyses of these three species show that 10a has the largest positive charge on the Fe atom about 0.50 electron. This is expected since its symmetry favors the back-donation from the d orbitals of the metal center into the π^* orbitals of N_2. On the other hand, the linear structure with end-on N_2 favors σ donation; then the charge on the Fe atom is small, about 0.18 electron. The 10b species has both types of N_2 bonding; therefore, it has an intermediate value for the charge on the Fe atom. The N−N frequencies follow the same trends. There are two N−N frequencies, one above 2000 cm^{-1} due to the end-on N−N stretch and another below 1850 cm^{-1} due to the side-on N−N stretch. The 10c species has frequencies at 2056 and 1800 cm^{-1}, 10a at 1812 and 1794 cm^{-1}, and the linear structure at 2136 and 2070 cm^{-1}.

Several different geometries have been optimized for the $Fe(N_2)_3$ complexes. However, we have not obtained any structure that lies close in energy to the end-on complex shown in Figure 2. The most stable is shown in Figure 11, which is 9.6 kcal mol^{-1} higher in energy than the ground state. It contains one side-on N_2 ligand and two end-on N_2 ligands. All other structures optimized are at least 18 kcal mol^{-1} higher in energy. The Fe−N bond distances are 1.985 and 1.854 Å for the side-on and end-on N_2 ligands, respectively. The N−N bond distances are 1.166 and 1.135 Å for the side-on and end-on N_2 ligands, respectively. The net charge on the Fe atom of 0.37 electron shows that the back-donation is enhanced with respect to the end-on species because of the presence of a side-on N_2 ligand. The calculated N−N frequencies are 1889.5, 2020.0, and 2421.1 cm^{-1}. The frequency of 2421.1 cm^{-1} is due to the symmetric N−N stretches of the end-on N_2 ligands. This large value can be explained by the fact that back-donation from d orbitals of the metal center to the π^* orbitals of the end-on ligands is smaller compared to that of the π^* orbitals of the side-on ligand. Consequently, the N−N bond of the end-on ligand is stronger, leading to the increase of its N−N frequency. The frequency 2020.0 cm^{-1} is due to the asymmetric N−N stretches of the end-on ligands, and the frequency of 1889.5 cm^{-1} is due to the N−N stretch of the side-on N_2 ligand.

Different starting geometries have been optimized to explore the potential energy surface of the $Fe(N_2)_4$ complex. We have optimized structures with one, two, three, and four side-on N_2 ligands at the singlet and triplet electronic states. Most of the triplets converged to the geometry shown in Figure 3. All the singlets converged to distinct local minima; however, they are at least 15 kcal mol^{-1} higher in energy than those of the end-on $Fe(N_2)_4$ complex.

Complexes with side-on N_2 ligands in equatorial and axial positions of pentacoordinated Fe−N_2 complexes have been used as starting geometries for optimization. All of them converged to the geometry shown in Figure 5. It is clear that $Fe(N_2)_5$ prefers the trigonal bipyramidal structure with end-on N_2 molecules.

Conclusions

$Fe(N_2)_n$ ($n = 1-5$) complexes have been studied with a density functional method. All the complexes have been optimized, and a vibrational analysis has been performed. The effects of the isotopically substituted complexes have been estimated for $Fe(N_2)_5$ and $Fe(N_2)_4$. FeN_2 is predicted to be linear. The interaction of Fe with the apolar molecule N_2 can be rationalized from the same molecular orbital picture used to describe FeCO and FeNO complexes.[30] However, the antibonding σ_{ab} orbital, due to the 5σ orbital of N_2 and the d_σ orbital of Fe, lies at lower energy, and therefore, it favors the high-multiplicity ground state. In fact, the triplet and quintet states are close in energy and the ground state is not unambiguously predicted. The binding energy is small with respect to those of the other complexes, about 8.8 kcal mol^{-1}. The dissociation energy of $Fe(N_2)_2$ is 27.7 kcal mol^{-1} larger than that of FeN_2. The increase in D_e is explained on the basis of the trans effect observed for this type of molecule. $Fe(N_2)_3$ is found to be planar with C_{2v} symmetry. Although the C_{3v} structure of $Fe(CO)_3$ has been reported, the optimized C_{3v} $Fe(N_2)_3$ is located 6.0 kcal mol^{-1} higher in energy than the C_{2v} structure. It has the largest dissociation energy of the series of complexes studied. $Fe(N_2)_4$ has been predicted to have a triplet ground state with C_{2v} symmetry, with the singlet with D_{2d} symmetry lying 4.1 kcal mol^{-1} higher in energy. However, its isoelectronic species $Fe(CO)_4$ has been predicted to have either D_{2d}[10] or C_{2v} symmetry[12] with a triplet ground state. It is important to note that there is experimental evidence that $Fe(CO)_4$ has C_{2v}[8] symmetry and is paramagnetic.[9] The saturated species $Fe(N_2)_5$ presents only small charges on the atoms. The metal center has a charge of 0.03 electrons compared to −0.5 electrons for $Fe(CO)_5$. The bonding of Fe to the N_2 ligands has been rationalized in terms of σ donation and π back-donation. The shape of the 5σ and π^* orbitals of N_2 is different from that of the CO and NO molecules, explaining the differences in geometry and ground states observed between the isoelectronic species $Fe(N_2)_n$ and $Fe(CO)_n$. The mean binding energy of $Fe(N_2)_5$ is predicted to be 22.5 kcal mol^{-1} smaller than that of $Fe(CO)_5$.

We have searched for side-on Fe−N_2 complexes in the potential energy surface. All of them are higher in energy than the end-on complexes with the exception of the side-on $Fe(N_2)_2$ complex which is 1.2 kcal mol^{-1} more stable than the end-on species. The end-on N_2 bonding is favored with increasing coordination number of the Fe−N_2 complexes.

The vibrational analysis ensures that all predicted ground states are minima on the potential energy surface, since all the frequencies are real. The infrared spectra of $Fe(N_2)_4$ and $Fe(N_2)_5$ are predicted to be similar at least in the range 1900−2300 cm^{-1}, and one cannot distinguish the two complexes in the nitrogen matrix. The effect of the isotopic substitution on the vibrational analysis has been described.

Acknowledgment. Financial support through grants from the Natural Sciences and Engineering Research Council (NSERC) of Canada, the National Research Council of Canada (joint NRC-NSERC program), the Fonds pour la formation des chercheurs et l'aide à la recherche (FCAR) of Québec, and the Fundação Coordenação de Aperfeiçoamento de Pessoal de Nível Superior (CAPES) of Brazil is gratefully acknowledged. We are grateful to the Services Informatiques de l'Université de Montréal for computing resources.

IC990066Z